Plasticity of Electrical Pacemaking by Interstitial Cells of Cajal and Gastric Dysrhythmias in *W/W^v* Mutant Mice

TAMÁS ÖRDÖG, MARJOLAINE BALDO, REKA DANKO, and KENTON M. SANDERS
Department of Physiology and Cell Biology, University of Nevada, Reno School of Medicine, Reno, Nevada

Background & Aims: Interstitial cells of Cajal (ICC) generate and propagate slow waves in the stomach. Gastric peristalsis depends on a proximal-to-distal gradient in slow wave frequency. We tested whether the gastric frequency gradient was an intrinsic property of ICC and whether dysrhythmias result from disruptions of ICC networks. *Methods:* We studied wild-type (WT) and *W/W^v* mice, which have only myenteric (pacemaker) ICC in the stomach. ICC distributions were analyzed by Kit immunofluorescence. Pacemaking in tissues was studied by intracellular electrophysiologic recording and in cultured ICC by monitoring mitochondrial [Ca^{2+}] oscillations with rhod-2 fluorescence or membrane potential with $DiBAC_4(3)$ fluorescence. *Results:* Slow wave frequencies were constant throughout WT gastric muscle sheets containing corpus and antrum. Separating the antrum from the corpus caused a significant drop in antral slow wave frequency. ICC from WT antrums also displayed significantly slower pacemaker frequencies than corpus ICC, but the corpus pacemaker frequency dominated in cocultures of corpus and antrum ICC. Myenteric ICC networks were reduced in *W/W^v* mice, particularly in the corpus. In *W/W^v* mice, separating the antrum from the corpus failed to reduce antral slow wave frequency. Antral pacemaker frequency in ICC from *W/W^v* stomachs was the same as in corpus ICC. *Conclusions:* The proximal-to-distal slow wave frequency gradient and entrainment of distal electrical activity by proximal pacemakers are fundamental properties of gastric ICC. Chronic depletion of ICC networks disrupts the proximal-to-distal frequency gradient, and emergence of ectopic pacemakers in the antrum may be caused by "reprogramming" of the ICC pacemaker apparatus.

Gastric emptying, particularly the emptying of solids, depends on peristaltic "rings" of contraction that spread from the orad corpus toward the pylorus.[1] This pattern of contractile activity is driven by propagating oscillations in membrane potential (slow waves).[2] Gastric slow waves originate from a dominant pacemaker site along the greater curvature in the orad corpus.[3] However, all regions of the gastric corpus and antrum are capable of generating spontaneous slow waves.[2,4] The intrinsic pacemaker frequency gradually decreases from the orad corpus to the pylorus (i.e., the proximal-to-distal gastric frequency gradient), and this can be demonstrated by recording slow waves from isolated regions of muscle removed from the corpus to the pylorus.[2–4] The orad corpus is the dominant pacemaker because it generates slow waves at the most rapid frequency.[3] Normally, there is high efficiency entrainment of distal pacemakers, and the dominant (fastest) slow wave frequency in the stomach is recorded at all sites as slow waves propagate from the corpus to the pylorus.[3,5–7]

Both the frequency and propagation of slow waves can change under pathologic circumstances. Gastric dysrhythmias, including bradygastrias (slower than normal rhythm), tachygastrias (faster than normal activity), and various arrhythmias,[8,9] can affect the normal pattern of slow wave propagation[5] and lead to antral hypomotility[10] and delayed gastric emptying.[8,9] Dysrhythmias may accompany a wide variety of conditions, including diabetic and idiopathic gastroparesis, functional dyspepsia, pregnancy, chronic mesenteric ischemia, gastric cancer, anorexia nervosa, motion sickness, unexplained nausea and vomiting, and abdominal surgery.[8,9,11] Aberrant gastric myoelectrical activity can be induced by various hormones, neurotransmitters, paracrine and autocrine mediators, drugs, and hyperglycemia,[5,9,12–15] and most investigators have focused on these factors as possible mediators of dysrhythmias. Chronic disorders, such as diabetes mellitus, chronic intestinal pseudo-obstruction, and aging,[9,16–18] might be accompanied by structural abnormalities that could contribute to the development of dysrhythmias, e.g., by sensitizing the pacemaker apparatus to a recurring arrhythmogenic stimulus.[9] So far, there have been few efforts to identify the fundamental mechanisms responsible for the gastric frequency gradi-

Abbreviations used in this paper: AU, arbitrary units; $[Ca^{2+}]_m$, mitochondrial $[Ca^{2+}]$; ICC, interstitial cell(s) of Cajal; IC-IM, intramuscular ICC; IC-MY, myenteric-region ICC; IC-SM, submucosal-border ICC; WT, wild type.

0016-5085/02/$35.00
doi:10.1053/gast.2002.37056

ent and structural and/or mechanistic abnormalities that might underlie abnormal electrical activity in chronic gastric motility disorders.

Interstitial cells of Cajal (ICC) in the region near the myenteric plexus (IC-MY) are the dominant pacemaker cells in the stomach,[19,20] and intramuscular ICC (IC-IM) are primarily mediators of neurotransmission.[21] Intact ICC networks are also required for the regenerative propagation of slow waves,[20,22] and structural damage to these cells or networks may lead to a variety of gastric motility disorders.[23–25] For example, we have recently reported that disruptions of gastric ICC networks cause loss of slow waves, interfere with slow wave propagation, and delay gastric emptying in nonobese, diabetic mice, a model of type 1 diabetes mellitus.[26] Partial disruption of ICC networks by blocking Kit signaling also resulted in spontaneous electrical arrhythmias, possibly because of the reduced coupling of residual ICC to the dominant pacemaker.[20]

In the present study, we investigated (1) whether the proximal-to-distal gastric frequency gradient is a fundamental property of corpus and antral ICC and (2) whether chronic disruption of ICC networks can lead to changes in pacemaker activity and dysrhythmias. For the latter purpose, we studied W/W^V mice because of the following: (1) Gastric emptying is delayed in these mice[27]; (2) W/W^V mice have only IC-MY in the stomach[21,28,29]; (3) preliminary studies indicated that IC-MY networks were also diminished in these animals; (4) ICC depletion in this model is due to genetic defects in c-*kit* that have no known direct effects on nerves or muscles of the *tunica muscularis*[23,24]; and (5) abnormalities in ICC network morphology are already in place at birth, permitting studies of isolated IC-MY networks in primary cell cultures.[30]

Materials and Methods

Animals and Tissue Preparation

Six-week-old WBB6F1/J-$Kit^W/Kit^{W\text{-}v}$ (W/W^V) mice and WBB6F1/J-*Kit*+/*Kit*+ wild-type (WT) controls were purchased from The Jackson Laboratory (Bar Harbor, ME). Nine- to fifteen-day-old W/W^V and WT mice were obtained from breeder pairs (WB/ReJ-*W*/+ females and C57BL/6J-W^V/+ males) also purchased from The Jackson Laboratory. W^V/+ and *W*/+ offspring, identified by their characteristic coat morphology,[31] were not used. Adult and 9- to 15-day-old BALB/c mice, used as additional controls, were obtained from breeder pairs purchased from Harlan Sprague-Dawley (Indianapolis, IN). Because data obtained in WBB6F1/J-*Kit*+/*Kit*+ WT and BALB/c mice were indistinguishable, the results were pooled (Kit+/+ control group). The animals were anesthetized by isoflurane inhalation (AErrane; Baxter Healthcare Corp., Deerfield, IL) and killed by decapitation. Mice were maintained and the experiments performed in accordance with the National Institutes of Health Guide for the Care and Use of Laboratory Animals, and all protocols were approved by the Institutional Animal Use and Care Committee at the University of Nevada, Reno, Nevada.

Stomachs were excised and opened along the lesser curvature. Gastric contents were washed away with Krebs–Ringer bicarbonate solution (composition below). The mucosa was removed by sharp dissection (adults) or peeling (9- to 15-day-old mice). The fundus was removed, and sheets consisting of the gastric corpus and antrum were used in subsequent steps. In stomachs opened along the lesser curvature, the incisura angularis was clearly recognizable on both sides of the tissue. When appropriate, the corpus and antrum were separated by cutting just distal to these indentations along a bundle of circular muscle. Corpus and antrum muscles were either used as whole sheets (electrophysiology and immunohistochemistry experiments) or processed for primary cell cultures by enzymatic dispersion.

Cell Cultures of Gastric Muscles

Gastric muscles consisting of the entire corpus and antrum or separated antral or corpus regions from 9- to 15-day-old mice were minced, equilibrated in Ca^{2+}-free Hank's solution (for composition see below) for 15 minutes and incubated, without agitation, at 37°C for 35 minutes in an enzyme solution containing collagenase (Worthington Type II; Worthington Biochemical Corp., Freehold, NJ; 1.3 mg/mL), bovine serum albumin (2 mg/mL), trypsin inhibitor (2 mg/mL), and adenosine triphosphate (0.27 mg/mL; all from Sigma, St. Louis, MO).[30] After 3 washes, the tissues were triturated through a series of 3 blunt pipettes of decreasing tip diameter. The resulting cell suspension was plated onto sterile 35-mm tissue culture dishes, the bottom of which had been replaced by No. 1 glass coverslips and coated with murine collagen (2.5 μg/mL; Collaborative Biomedical Products, Bedford, MA). Cells were cultured at 37°C in a 5% CO_2 incubator in Smooth Muscle Growth Medium 2 (BioWhittaker Inc., Walkersville, MD), supplemented with 2% antibiotic/antimycotic (GIBCO BRL, Gaithersburg, MD) and murine stem cell factor (20 ng/mL; Sigma). The medium was changed after 24 hours to Smooth Muscle Growth Medium 2 containing stem cell factor without antibiotic/antimycotic. Cultures were used 4–5 days after plating.

To test whether both antrum and corpus ICC were present in cultures prepared from combined corpus and antrum muscles, cells were also dispersed separately from the corpus and antrum. These were sedimented by centrifugation (300*g*, 5 minutes, 4°C) and labeled separately with the cell-tracking dyes SP-$DiOC_{18}$(3) (corpus) and SP-$DiIC_{18}$(3) (antrum) (Molecular Probes, Eugene, OR; 2 μmol/L, 5 minutes at 37°C, then 15 minutes at 4°C). After labeling, the cells were washed, thoroughly mixed, and cultured as described previously. After 4–5 days, the cultures were fixed with 4% paraformaldehyde

saline (pH 7.4, 10 minutes at room temperature) and treated with acetone (10 minutes, 4°C).

Kit Immunohistochemistry

ICC were identified with antibodies to the receptor tyrosine kinase Kit (ACK2, monoclonal rat anti-mouse IgG) as described previously.[20,30] Whole mounts of gastric tissues and cell cultures were fixed with cold acetone. Nonspecific antibody binding was reduced by incubation in 1% (wt/vol) bovine serum albumin (Sigma) in phosphate-buffered saline (10 mmol/L; pH 7.4) for 1 hour at room temperature. Specimens were incubated with ACK2 (5 μg/mL) at 4°C for 48 hours (tissues) or overnight (cells). In tissues, 0.3% (vol/vol) Triton X-100 (Sigma) was used to facilitate the penetration of the primary antibody. Immunoreactivity was detected with a secondary antibody conjugated with Alexa Fluor 488 (anti-rat IgG; Molecular Probes; 10 μg/mL). As controls, the primary or the secondary antibodies were omitted from the incubation solutions.

Imaging of Histologic Specimens

Kit-like immunoreactivity was examined with a Bio-Rad MRC 600 confocal microscope (Hercules, CA) equipped with an Ar-Kr laser and coupled to a Nikon Diaphot (Nikon Instruments, Melville, NY) inverted microscope. Images were acquired with Nikon Fluor 40×/1.30 NA (tissues) or Nikon PlanApo 60×/1.40 NA (cells) oil immersion objectives using an excitation wavelength of 488 nm. The confocal micrographs in this manuscript are digital composites of Z-series scans constructed with CoMOS software (version 7.0a; Bio-Rad). Phase-contrast and wide-field fluorescent images of cell cultures were acquired with a Leitz Wetzlar Diaplan microscope equipped with a PL Fluotar 40×/0.70 NA objective, a Hg arc lamp, and a Leica LEI-750 color camera (Leica Microsystems, Wetzlar, Germany). Images were digitized with Matrox Meteor Driver and MetaMorph 3.0 software (Universal Imaging Corp., West Chester, PA). Additional wide-field fluorescent images were acquired with a Leica DMRX microscope, HC PL APO 20×/0.70 NA objective, DC 500 digital camera, and IM 1000 software (Leica Microsystems, Wetzlar, Germany).

Quantitative Analysis of IC-MY Densities

Counting of IC-MY in whole-mounts of the murine gastric antrum was not possible because of the very high densities of cell bodies and processes.[28] In the present study, we compared cell densities in whole mounts of W/W^V and Kit+/+ stomachs by using a technique modified from He et al.[32] Briefly, cellular and background fluorescence were separated by thresholding on the peak of the distribution of cellular fluorescence in 2-dimensional composites of confocal sections representing the entire thickness of the myenteric region. To eliminate differences in brightness among different cells, cell bodies, and processes, fluorescence values above and below the threshold were assigned 255 and 0 (the extremes of the 8-bit gray scale), respectively. Cell densities were then expressed as mean pixel intensities over a standard area (289 × 193 μm). All image analysis was performed with Corel Photo-Paint 7.373 (Corel Corp., Ottawa, Ontario, Canada).

Electrophysiology

Intact gastric tissues consisting of gastric corpus and antrum were pinned, with the circular muscle facing upward, onto the surface of a dish coated with Sylgard 184 silicone elastomer (Dow Corning Corp., Midland, MI) and perfused with oxygenated Krebs-Ringer bicarbonate solution warmed to 37.5°C ± 0.5°C. Circular muscle cells were impaled with glass microelectrodes filled with 3 mol/L KCl with resistances of 40–100 MΩ as described previously.[20] Transmembrane potentials were measured with a standard microelectrode amplifier (Intra 767; World Precision Instruments, Sarasota, FL) and recorded on computer files using a BIOPAC MP100 data acquisition system (BIOPAC Systems, Santa Barbara, CA). Recordings were performed from multiple sites along the circumference and the longitudinal axis of both the corpus and the antrum. Then the corpus and antrum were cut apart as described previously, and further impalements were made in the disconnected tissues. In the text, the number of cells from which recordings were made is denoted by "n." The number of tissues from which the "n" was obtained is also provided.

Fluorescent Imaging of Pacemaker Activity in Cultured ICC

To monitor mitochondrial $[Ca^{2+}]$ ($[Ca^{2+}]_m$), cells were loaded with 4.4 μmol/L reduced rhod-2 AM, prepared according to the manufacturer's recommendations (Molecular Probes), in a HEPES-buffered physiologic salt solution (for composition see below) containing 5% fetal bovine serum (HyClone, Logan, UT) for 1 hour at 4°C. Loaded cells were cultured for an additional 6–18 hours in phenol red-free medium 199 (Sigma) containing 5% fetal bovine serum to ensure complete elimination of the dye from the cytoplasm.[33,34] Some cultures were coloaded with MitoTracker Green FM (Molecular Probes; 100 nmol/L in medium 199; 35 minutes at 37°C), a dye that binds covalently to the inner mitochondrial membrane and fluoresces independently of $[Ca^{2+}]_m$ and membrane potential, thus providing an independent test of mitochondrial localization and specificity of rhod-2 fluorescence. The colocalization of rhod-2 and MitoTracker Green was studied by confocal microscopy utilizing excitation at 568 nm and 488 nm, respectively.[33] Time-series experiments were performed in HEPES-buffered physiologic salt solution warmed to 29°C ± 0.5°C. $[Ca^{2+}]_m$ oscillations associated with electrical pacemaking in ICC were monitored by using the line-scan option of the Bio-Rad MRC 600 (acquisition rate: 4.2 Hz; excitation wavelength: 568 nm) as described previously.[33] Traces were smoothed off-line by adjacent averaging using Microcal Origin 4.1 (Microcal Software, Inc., Northampton, MA).

In separate experiments, slow wave depolarizations were monitored in cultured ICC directly with bis-(1,3-dibutylbarbituric acid)trimethine oxonol ($DiBAC_4(3)$; Molecular Probes).

This anionic dye binds to intracellular membranes and proteins and exhibits increased fluorescence upon cell depolarization.[35] $DiBAC_4(3)$ was added to the HEPES-buffered superfusion buffer at a final concentration of 1 μmol/L.[35] The response of the dye to depolarization was verified by increasing external $[K^+]$ from 5 to 135 mmol/L (data not shown). To achieve better temperature control (29°C ± 0.5°C) than was possible with the confocal line scanning microscopy, which uses high-intensity laser light, time-series experiments were performed using a wide-field video fluorescence imaging system (Ionoptix Corp., Milton, MA) coupled to a Nikon Diaphot inverted microscope equipped with a 40×/1.3 NA oil-immersion objective and an appropriate filter set (Omega Optical, Inc., Brattleboro, VT). A xenon lamp was used as the light source, and an intensified CCD camera collected fluorescence. Video signals were digitized at 55 Hz, averaged to a final acquisition rate of 5 Hz with the aid of IonWizard (version 4.4; Ionoptix) software and analyzed as described previously.

Solutions

Concentrations are given in mmol/L. Krebs–Ringer bicarbonate solution: 120.35 NaCl, 5.9 KCl, 2.5 $CaCl_2$, 1.2 $MgCl_2$, 15.5 $NaHCO_3$, 1.2 NaH_2PO_4, 11.5 glucose, pH 7.3–7.4 when bubbled with 97% O_2 and 3% CO_2. Ca^{2+}-free Hank's solution: 125 NaCl, 5.36 KCl, 15.5 $NaHCO_3$, 0.336 Na_2HPO_4, 0.44 KH_2PO_4, 10 glucose, 2.9 sucrose, and 11 HEPES adjusted to pH 7.2 with NaOH. HEPES-buffered physiologic salt solution: 135 NaCl, 5 KCl, 2 $CaCl_2$, 1.2 $MgCl_2$, 10 glucose, and 10 HEPES, adjusted to pH 7.4 with Tris.

Statistical Analyses

The SigmaStat Statistical Software for Windows Version 2.03 (SPSS Science, Chicago, IL) was used for all statistical analyses. The frequency of slow waves or $[Ca^{2+}]_m$ oscillations was calculated from the mean interevent interval for the particular recording. Distribution of these frequency data was then characterized by histograms using a bin size of 0.5 cycle/minute. The Kolmogorov–Smirnov test with Lilliefors' correction was used to test values for normality of the estimated underlying population. Data following normal and skewed distribution were described by mean ± SD and median (25th percentile, 75th percentile), respectively. In W/W^V tissues, similar to ACK2-treated[20] and diabetic stomachs,[26] the reduction in ICC density resulted in focal losses of slow waves. Because the purpose of this study was to analyze residual activity, impalements not yielding slow waves were excluded from frequency analysis. Slow waves with a sustained frequency exceeding the group mean plus 3 SD were statistical outliers; these rare events were considered "cellular-level tachygastrias" and were also excluded from further frequency analysis. Before performing tests of significance, data were examined for normality and equal variance to determine whether parametric or nonparametric tests should be used. Unpaired Student t test and Kruskal–Wallis 1-way ANOVA on ranks followed by all-pairwise multiple comparison (Dunn's method) were used for statistical comparisons. A probability value of $P < 0.05$ was used as a cutoff for statistical significance in all statistical procedures.

Results

Role of ICC in the Proximal-to-Distal Slow Wave Frequency Gradient and Entrainment

Experiments were performed to determine whether the proximal-to-distal gastric frequency gradient common to other mammalian species occurs in the mouse.[2–4] Intracellular electrophysiologic recordings were made from cells of the corpus and antrum of 9

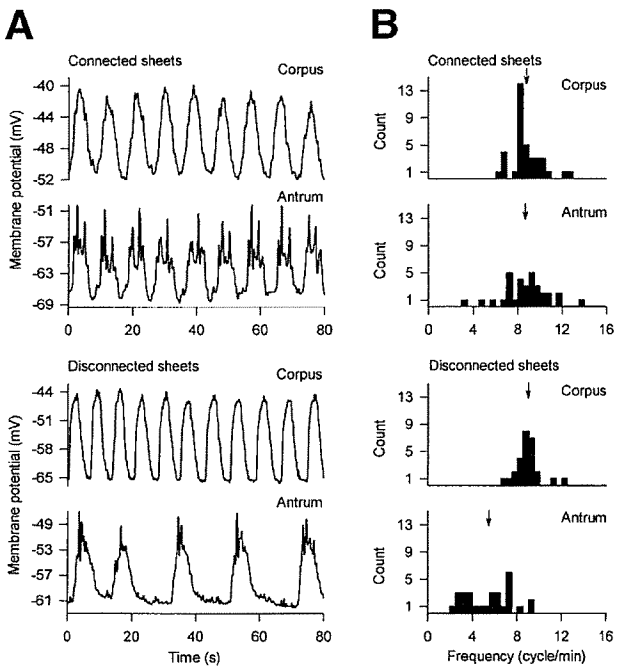

Figure 1. Frequency of electrical slow wave activity in the corpus and antrum of Kit+/+ mice before and after disconnection. (*A*) Representative intracellular recordings made in the gastric corpus and antrum before and after disconnection of the 2 regions. Antral slow waves had faster upstrokes, longer plateau potentials, and a higher probability of having superimposed spikes than slow waves in the corpus. (*B*) Histogram analysis of slow wave frequencies, in which each observation represents the mean frequency during a single impalement. In 2 impalements from 1 corpus muscle, slow wave frequencies of 15.1 and 15.4 cycle/min were recorded. In 2 impalements of 2 disconnected antrums, slow wave frequencies of 35.4 and 18.0 cycle/min were recorded. These were statistical outliers and considered "cellular-level tachygastrias," and they were excluded from the histograms and analyses (see Materials and Methods section; also, note that such frequencies were rare because we found only 6 in 256 impalements). Group means are indicated by *arrows* in the histograms and were as follows (±SD): connected corpus, 8.76 ± 1.40 cycle/min, n = 37; connected antrum, 8.69 ± 2.12 cycle/min, n = 32; disconnected corpus, 8.93 ± 1.09 cycle/min, n = 27; disconnected antrum, 5.43 ± 2.03 cycle/min, n = 29. Note that antral slow wave frequency decreased significantly after separation from the dominant pacemaker in the corpus ($P < 0.001$ by Kruskal–Wallis 1-way ANOVA on ranks followed by Dunn's all-pairwise multiple comparison).

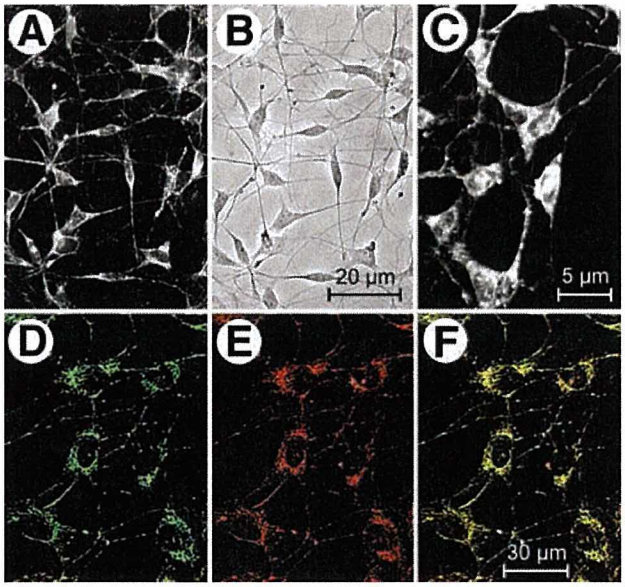

Figure 2. Kit-like immunoreactivity, $DiBAC_4(3)$, and rhod-2 fluorescence in ICC cultured from gastric muscles. (*A* and *B*) Wide-field fluorescent (*A*) and phase-contrast (*B*) images of the same Kit+/+ ICC network. Note that the characteristic morphology of Kit+ gastric ICC (fusiform cells or triangle-shaped cell bodies with multiple, slender processes forming dense interconnections) was distinctive and permitted their identification without immunostaining. Similar 2-dimensional networks, indistinguishable from those obtained from cultures of Kit+/+ cells, were observed in cultures of W/W^v cells, suggesting that these networks were formed by IC-MY cells (i.e., because W/W^v stomachs lack IC-IM and IC-SM). (*C*) Confocal image showing $DiBAC_4(3)$ fluorescence in an ICC network. $DiBAC_4(3)$ was mainly localized in the cytoplasm, in which its fluoresence increased in response to depolarization. (*D–F*) Confocal images demonstrating mitochondrial localization of rhod-2. Dense clusters of mitochondria were labeled with MitoTracker Green FM in the perinuclear region and within processes (*D*). Rhod-2 fluorescence (*E*) overlapped with MitoTracker Green FM as indicated by *yellow* in the overlaid images (*F*). (*Bar* in *B* for *A*, *B;* in *F* for *D–F*.)

Kit+/+ controls (5 WT and 4 BALB/c mice) before and after physical disconnection of the corpus and antrum. All impalements (n = 129) yielded regular slow wave activity with an average resting membrane potential (i.e., most negative potential between slow waves) of -55 ± 12 mV. In intact sheets, slow wave frequencies were the same in the antrum and corpus (Figure 1, *Connected sheets*). Slow-wave frequency in the corpus was not significantly affected by disconnecting the antrum (Figure 1, *Disconnected sheets*). In contrast to the corpus, disconnection of the corpus had profound effects on the slow wave frequency in the antrum. Immediately after cutting the tissue, slow waves were arrhythmic. After 10–30 minutes, slow waves stabilized, and the frequency of slow waves was significantly depressed as compared with intact corpus and antral sheets (Figure 1).

Next, we tested whether the gastric frequency gradient was an intrinsic feature of ICC by recording spontaneous activity of ICC isolated separately from the corpus and antrum of 11 Kit+/+ mice.[30,33] We also tested whether entrainment of distal electrical activity could take place in cell culture by studying pacemaker activity in cocultured corpus and antrum ICC. ICC in culture were identified by immunofluorescence using antibodies to Kit, a specific marker for these cells (see details in Figure 2*A* and *B*).[21,23–25]

In the first set of experiments, pacemaker activity of IC-MY was studied by monitoring oscillations in $[Ca^{2+}]_m$ visualized by rhod-2 fluorescence.[33] Mitochondrial localization of rhod-2 was verified by colabeling with MitoTracker Green FM[33] (Figure 2*D–F*). Monitoring of Ca^{2+}-dependent fluorescence of rhod-2 in IC-MY revealed rhythmic oscillations in $[Ca^{2+}]_m$ in all experi-

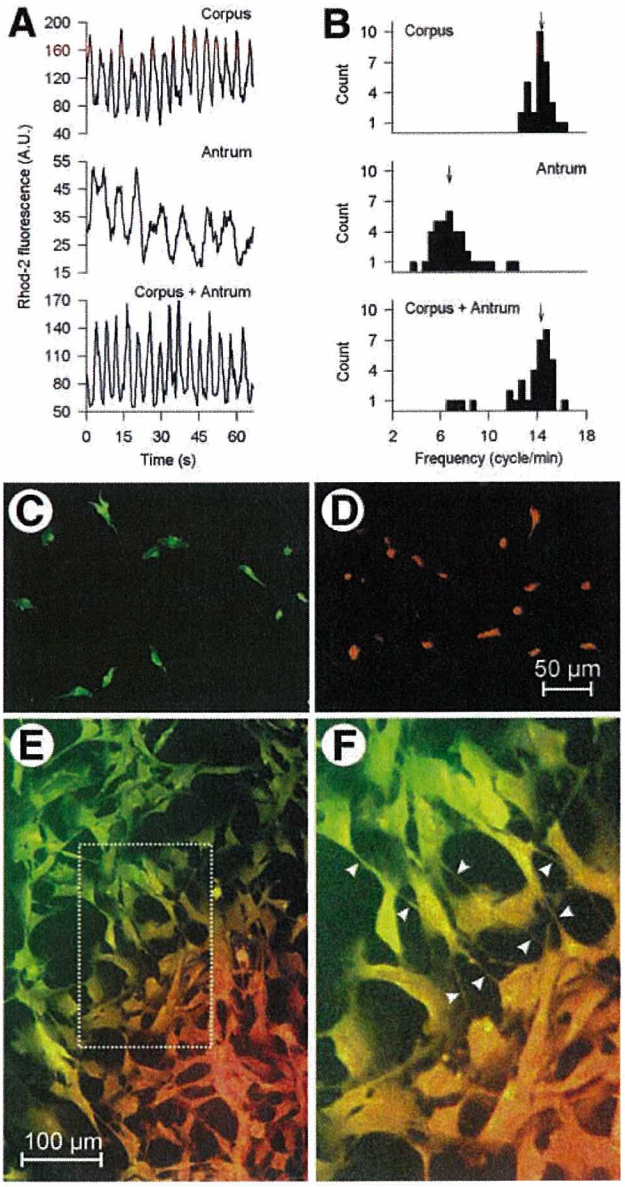

mental groups. $[Ca^{2+}]_m$ transients in antral ICC of Kit+/+ mice had significantly slower rhythms than IC-MY from the corpus (Figure 3*A* and *B*). In cultures prepared from the entire corpus and antrum, the higher frequencies of corpus ICC dominated (Figure 3*A* and *B*). To ensure that the dominance of corpus frequencies was not due to the absence of antrum ICC in mixed cultures, cells were dispersed separately from the corpus and antrum, labeled with the cell-tracking dyes SP-$DiOC_{18}(3)$ (corpus; Figure 3*C*) and SP-$DiIC_{18}(3)$ (antrum; Figure 3*D*), and cultured together. Clonal proliferation in these cultures gave rise to clusters of antrum and corpus ICC that retained specific labeling for 4–5 days (Figure 3*E*). Corpus and antrum ICC were both represented in these cultures and formed common networks with nearby clusters of cells connected by intercellular processes (Figure 3*F*).

In experiments using confocal microscopy, gastric pacemaker frequencies were higher than obtained in electrophysiologic recordings. Because slow wave generation depends upon metabolic factors,[33] it is possible that heating because of illumination by the laser might enhance pacemaker frequency. Thus, we conducted separate experiments using wide-field fluorescence and a low-intensity xenon light source. In these experiments, we utilized the membrane potential-sensing dye $DiBAC_4(3)$ to directly monitor membrane potential oscillations. Lower frequency slow waves were recorded with this technique, but the activity pattern was the same as with confocal microscopy. For example, the median (25th percentile, 75th percentile) frequency of slow waves in the corpus ICC was 3.90 (2.22; 5.36) cycle/min (n = 134), and this was not different from the mixed (corpus and antrum) ICC cultures [i.e., 4.37 (3.37; 5.29) cycle/min, n = 94]. Antral ICC displayed significantly slower activity: 0.83 (0.71; 1.05) cycle/min (n = 44; $P < 0.001$; Kruskal–Wallis 1-way ANOVA on ranks followed by Dunn's all-pairwise multiple comparison). This frequency was similar to the frequency of spontaneous pacemaker currents recorded from antral ICC by the patch-clamp technique at the same temperature (1.0 ± 0.2 cycle/min, 29°C).[30]

Figure 3. Oscillations in mitochondrial $[Ca^{2+}]$ in ICC cultured from the corpus and antrum of Kit+/+ mice. (*A*) Representative recordings in pacemaker ICC of oscillations in mitochondrial rhod-2 fluorescence, expressed in arbitrary units (AU) on an 8-bit scale. These oscillations reflect, and are closely associated with, the rhythmic inward current that underlies electrical slow waves.[33] (*B*) Histogram representation of frequencies of $[Ca^{2+}]_m$ oscillations. *Arrows* signify group medians, which were as follows: corpus cells, 14.42 (13.99; 14.64) cycle/min (median, [25th percentile; 75th percentile]; note that this method of data presentation was used because one of the data sets in this study did not follow a Gaussian distribution [$P < 0.025$; Kolmogorov–Smirnov test]), n = 31; antrum cells, 6.74 (5.65; 7.86) cycle/min, n = 38; cocultured corpus and antrum cells, 14.34 (12.82; 14.71) cycle/min, n = 36. A significantly slower frequency was found in antrum ICC than in ICC from the corpus, and the higher frequencies characteristic of corpus ICC dominated in cells prepared from the entire corpus and antrum ($P < 0.001$; Kruskal–Wallis 1-way ANOVA on ranks followed by Dunn's all-pairwise multiple comparison). (*C* and *D*) Cells freshly dispersed from the *tunica muscularis* of the corpus (*C*) and antrum (*D*) and labeled with the cell-tracking dyes SP-$DiOC_{18}(3)$ (*green*) and SP-$DiIC_{18}(3)$ (*red*), respectively. (*E*) Clonal proliferation in cocultures of corpus and antrum cells gave rise to clusters of IC-MY from both regions of the stomach. Connections between a cluster of corpus ICC (*green*) and antrum ICC (*red*) are indicated by *arrowheads* in *F*, which is an enlargement of the area outlined in *E*. *Yellow* or *orange* color of cells located at the interface of conjoined clusters results from simultaneous illumination by the *green*- and *red*-emitting dyes in the nearby cells.

Can Gastric Dysrhythmias Result From Disruptions of ICC Networks?

We studied the morphology of gastric ICC networks in Kit+/+ (7 WT and 4 BALB/c tissues) and W/W^V (n = 9) mice by qualitative and quantitative immunohistochemistry using antibodies to Kit, a specific marker for these cells.[21,23–25] As previously reported, Kit-like immunoreactivity in Kit+/+ stomachs was found in the myenteric region (IC-MY) between bundles of muscle cells (IC-IM) and along the submucosal surface of the circular muscle layer (IC-SM).[20,23,28,29,36] IC-IM and IC-SM were missing from W/W^V stomachs.[21–23,29,37] Although IC-MY were present in both the W/W^V corpus and the antrum, the density and morphology of the IC-MY networks were profoundly altered relative to the Kit+/+ control animals (Figures 4–6).

In Kit+/+ mice, IC-MY formed a continuous network throughout the corpus and antrum. The density of IC-MY networks increased along the longitudinal axis from the corpus to the distal antrum and decreased along the gastric circumference from the greater curvature to the lesser curvature (Figure 4; Figure 6*A*, *left*). IC-MY were nonexistent in the cardia and sparse in a narrow band of tissue along the lesser curvature from the cardia to the pylorus (Figure 4*C*, *F*, and *I*; *white* and *light gray* in Figure 6*A*, *left*).

In W/W^V stomachs, IC-MY networks were more dense in the antrum than in the corpus and along the greater curvature than the lesser curvature as in Kit+/+ stomachs (Figure 5; Figure 6*A*, *right*). However, the regional differences in IC-MY densities noted in Kit+/+ mice were amplified in W/W^V mice. IC-MY were closest to normal density in the greater curvature of the distal antrum (compare Figure 5*G* with Figure 4*G*), in which quantitative image analysis (Figures 6*B* and *C*) did not reveal a statistically significant difference from Kit+/+ controls (Figure 6*C*, *panel 3*). However, the density of

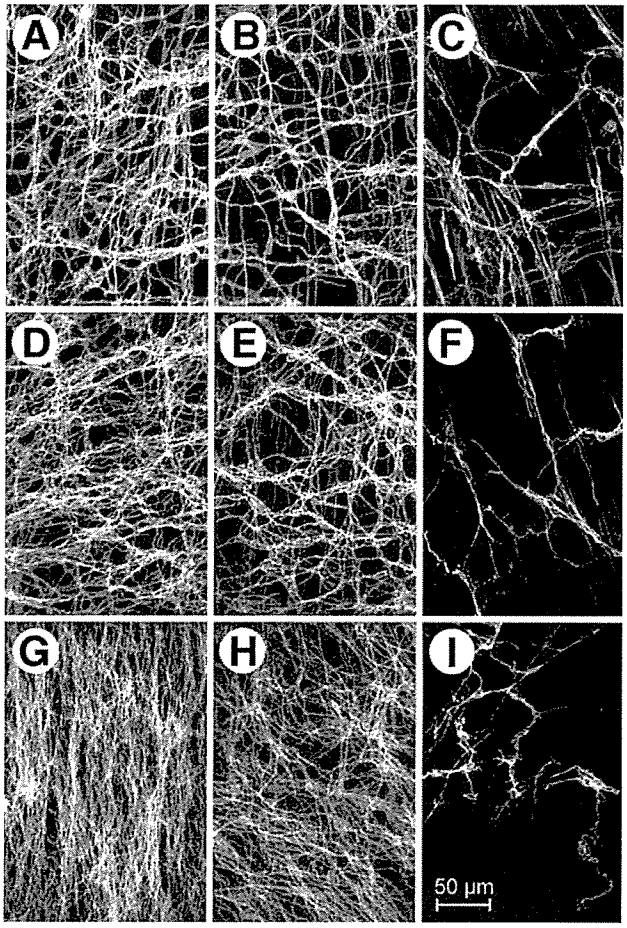

Figure 4. Changes in the density of myenteric ICC networks along the longitudinal axis and circumference of the stomach of Kit+/+ mice. Optical sections representing the myenteric region of WT mice are shown. The areas from which the images were taken are indicated in the left half of Figure 6*A* by lettering that corresponds to the lettering in this figure. Note the gradual decline in IC-MY density from the distal antrum (*bottom panels*) toward the orad corpus (*top panels*) and from the greater curvature (*left panels*) toward the cardia (*C*) and the lesser curvature in the antrum (*F* and *I*). Despite the lower density of IC-MY near the lesser curvature, this portion of the IC-MY network appeared to form a continuous network with the higher density regions of IC-MY. (*Bar* in *I* for all panels.)

IC-MY was significantly less than normal in the greater curvature of the orad corpus (Figure 6*C*, *panel 1*; also compare Figure 5*A* with Figure 4*A*) and in areas corresponding to the abdominal and dorsal surfaces of the orad corpus (Figure 6*C*, *panel 2*) and the distal antrum (Figure 6*C*, *panel 4*). In addition, IC-MY in W/W^V mice tended to collect in "bundles" (compare *panels A*, *B*, *D*, and *E* in Figures 4 and 5), which frequently ended abruptly, particularly in the antrum (Figure 5*H*), leaving small groups of IC-MY cells isolated from the denser parts of the network (Figure 5*C*, *F*, and *I*).

Next, we studied the effects of ICC network disruptions on the proximal-to-distal gastric frequency gradient in 7 W/W^V mice by repeating the intracellular electrophysiologic experiments described for Kit+/+ animals above (see Figure 1). We did not record slow waves in a significant number (27%) of circular muscle cells in W/W^V stomachs in contrast to the ubiquitous recording of slow waves in control tissues. The tendency for quiescence in cells of W/W^V stomachs increased near the lesser curvature, in which IC-MY density was reduced (see Figures 5 and 6 and note similar observations

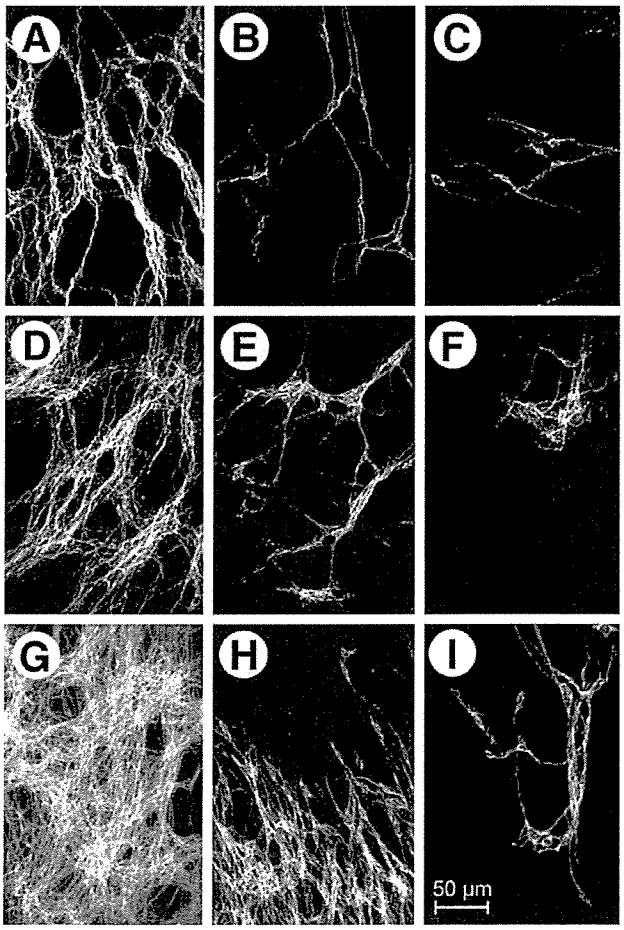

Figure 5. Changes in the density of myenteric ICC networks along the longitudinal axis and circumference of the stomach of W/W^V mice. Optical sections of the myenteric region in W/W^V mice are shown. The areas from which the images were taken are indicated in the right half of Figure 6*A* by lettering that corresponds to the lettering in this figure. Although the general trends in IC-MY density were similar to those observed in Kit+/+ mice, there was a more precipitous drop in IC-MY density along both the longitudinal and circumferential axes. For example, the density in the orad corpus (*A*) was more reduced than in the distal antrum (*G*). IC-MY also tended to form "bundles" throughout the stomach and occurred in "islands" along the lesser curvature (*right panels*). Panel *H* (where the top of the panel represents the lateral border of the image) shows a tendency for dense IC-MY networks to end abruptly. Islands of IC-MY cells in regions closer to the lesser curvature were not in contact with the main ICC network. (*Bar* in *I* for all panels.)

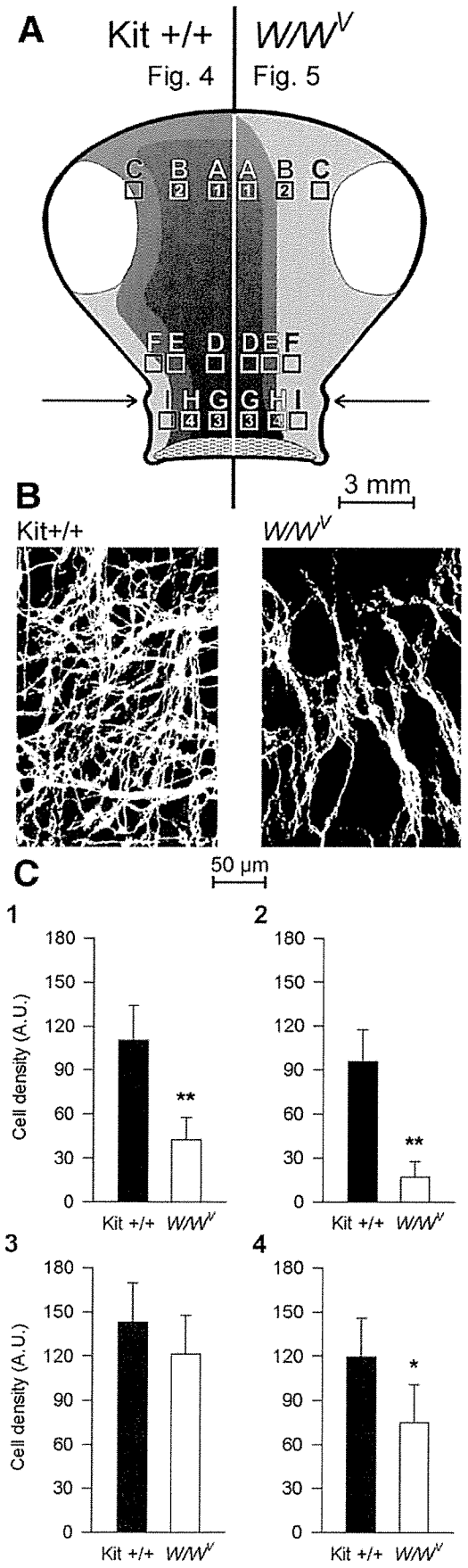

in Ördög et al.[20] and Ördög et al.[26]). When slow waves were present in W/W^V tissues (n = 127), resting membrane potentials averaged -59 ± 12 mV. Slow wave frequencies in intact sheets were not statistically different from slow wave frequencies in Kit+/+ tissues ($P > 0.05$; Kruskal-Wallis 1-way ANOVA on ranks; compare *Connected sheets* in Figures 1 and 7). When the corpus was separated from the antrum in W/W^V stomachs, the frequency of slow waves in the corpus did not change (Figure 7). In contrast to the dramatic decrease in antral slow wave frequency in Kit+/+ stomachs when the corpus was removed, we did not observe a change in antral slow wave frequency after separating antrum from corpus in W/W^V stomachs, i.e., slow waves occurred at the same frequency as the dominant pacemaker (corpus) activity (Figure 7, *bottom panels*). Antral frequency remained elevated for several hours at levels that were statistically indistinguishable from the frequency of the antrum and corpus in intact gastric sheets. The frequency of antral slow waves in W/W^V stomachs after disconnecting the corpus and antrum was statistically higher than the frequency of slow waves in Kit+/+ antrums that were separated from the corpus ($P < 0.001$; compare *bottom panels* in Figures 1 and 7).

Figure 6. Qualitative and quantitative analysis of myenteric ICC densities in the stomachs of Kit+/+ and W/W^V mice. (*A*) Cartoon represents the densities of IC-MY in stomachs of Kit+/+ (*left half*) and W/W^V (*right half*) mice. The cartoon depicts the corpus and antrum of a stomach opened along the lesser curvature and stretched flat for immunohistochemistry. *Top*: corpus-fundus border; *Bottom*: pyloric sphincter. The *crosshatched* area represents tissues just orad to the gastroduodenal junction. IC-MY networks in this region had a complicated morphology characteristic of the pylorus.[29] This area was not studied in the present work. Changes in shading signify different densities of IC-MY networks, with *darker tones* corresponding to the highest densities. *White areas* correspond to the cardia and indicate a complete lack of IC-MY in that region. *Squares* labeled with capital letters indicate the positions of actual confocal images from the myenteric regions of Kit+/+ (*left*) and W/W^V mice (*right*) shown in Figures 4 and 5, respectively. *Numbers* inside some of the *squares* signify the positions of the images used to obtain ICC densities shown in *C*. *Arrows* indicate the position of the cuts placed just aborad to the incisura angularis to separate the corpus and the antrum in the electrophysiology and cell culture experiments. (*B*) Representative images illustrating the threshold-based conversion of *gray-scale* images to binary (*black* and *white*) ones for quantitative assessment. The images correspond to the *A* panels (orad corpus, greater curvature) of Figures 4 (Kit+/+) and 5 (W/W^V), respectively. (*C*) Comparisons of cell densities (mean ± SD), obtained by averaging the *black* and *white* pixels in the converted images and expressed as arbitrary units (AU) on an 8-bit scale in selected regions of Kit+/+ (*solid bars*) and W/W^V (*open bars*) stomachs. Numbering of bar graphs corresponds to the numbering of squares in *A* to indicate the areas analyzed. Note that, with the exception of the distal antrum in the vicinity of the greater curvature, IC-MY densities were significantly reduced in W/W^V stomachs (**$P < 0.001$; *$P < 0.004$; unpaired Student *t* tests). (*Bar* in *B* for both panels.)

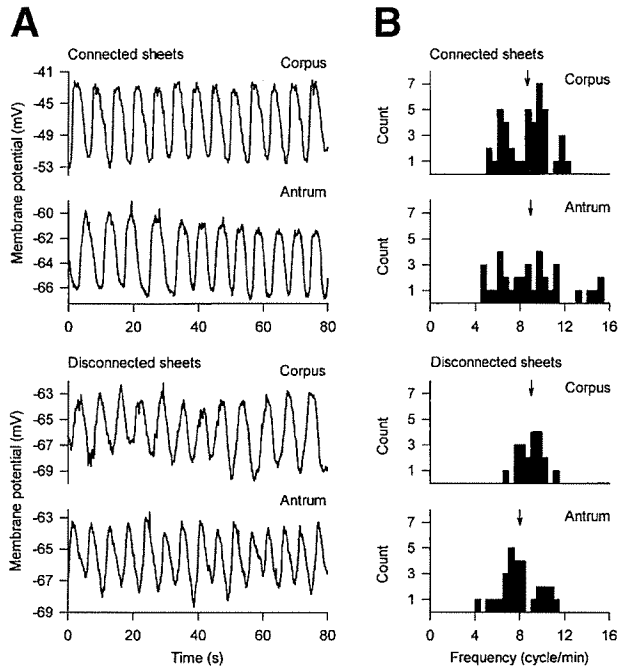

Figure 7. Frequency of electrical slow wave activity in the corpus and antrum of W/W^V mice before and after disconnection. (*A*) Intracellular recordings made from the corpus and antrum before and after disconnection of these regions. In the W/W^V tissues, antral slow waves did not have the characteristic plateau with superimposed spikes and were similar in waveform to slow waves in the corpus. (*B*) Histogram analysis of slow wave frequencies, in which each observation represents the mean frequency in a single impalement. Group means are indicated by *arrows* in the histograms and were as follows (±SD): connected corpus, 8.68 ± 1.94 cycle/min, n = 42; connected antrum, 8.98 ± 3.06 cycle/min, n = 35; disconnected corpus, 9.02 ± 1.06 cycle/min, n = 20; disconnected antrum, 8.02 ± 1.73 cycle/min, n = 28. Impalements not yielding slow waves were not analyzed. Recordings with rapid slow wave frequencies (1 cell in the connected corpus: 19.0 cycle/min; and 1 cell in a disconnected antrum: 20.5 cycle/min) were also not included in the histograms. No statistically significant differences were found among the groups shown in *B* ($P > 0.05$; Kruskal–Wallis 1-way ANOVA on ranks).

To test whether the increased slow wave frequency in the antral muscles isolated from W/W^V stomachs was due to a change in the intrinsic pacemaker cells, we studied the spontaneous activity of cultured ICC isolated separately from the corpus and antrum of 7 W/W^V mice using rhod-2 fluorescence (see *control experiments* in Figure 3*A* and *B*). As observed in intact W/W^V muscles, the frequency gradient between ICC from corpus and antrum was lost in W/W^V cultures. The frequencies of $[Ca^{2+}]_m$ oscillations in IC-MY cultured from W/W^V corpus and antrum were statistically indistinguishable from each other and from cocultured corpus and antrum ICC (Figure 8). The frequency of $[Ca^{2+}]_m$ oscillations in all W/W^V cells was not different from corpus ICC from Kit+/+ tissues ($P > 0.05$) but was significantly greater than the frequency in antral ICC from Kit+/+ animals ($P < 0.001$; all analyses by Kruskal-Wallis 1-way ANOVA on ranks followed by Dunn's all-pairwise multiple comparison; compare panels *A* and *B* in Figures 3 and 8).

Discussion

Previous studies have shown that ICC generate gastric slow waves.[19,20] In this study, we have shown that the gastric slow wave frequency gradient, a critical feature of the gastric myogenic regulation that ensures proximal-to-distal spread of slow waves and gastric peristaltic waves, is an intrinsic property of the ICC that populate proximal and distal muscular regions. The cellular factors responsible for the frequency gradient are preserved in cultured ICC from corpus and antral muscles. Future studies may unravel the specific cellular mechanisms in ICC that are responsible for the differences in pacemaker frequency. Coupling of corpus pacemakers with antral pacemakers leads to entrainment such that slow waves spread from the dominant (corpus) pacemaker to the pylorus in the normal stomach.[3] We found that faster, corpus ICC couple with slower, antral ICC in

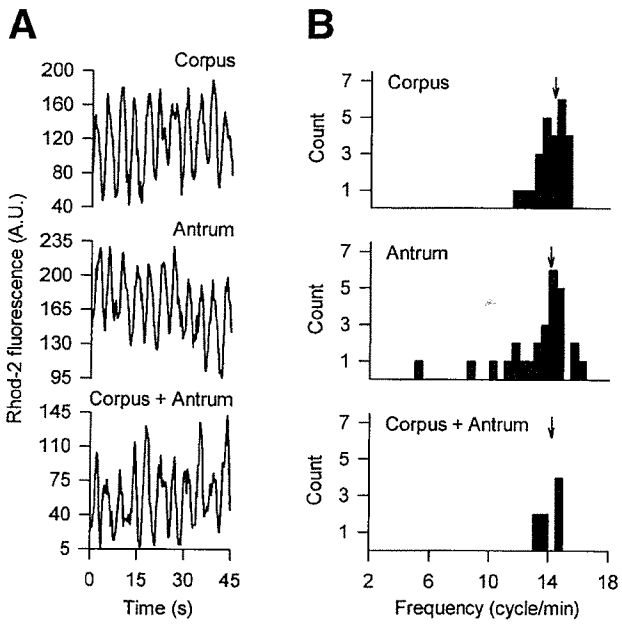

Figure 8. Oscillations in mitochondrial $[Ca^{2+}]$ in ICC cultured from the corpus and antrum of W/W^V mice. (*A*) Representative recordings of oscillations in $[Ca^{2+}]_m$ in ICC cultured from W/W^V tissues. (*B*) Histogram representation of frequencies of oscillations in mitochondrial rhod-2 fluorescence. *Arrows* indicate group medians, which were as follows: corpus cells, 14.34 (13.49; 14.85) cycle/min [median (25th percentile; 75th percentile)], n = 25; antrum cells, 14.08 (12.51; 14.57), n = 27; cocultured corpus and antrum cells, 14.17 (13.53; 14.60) cycle/min, n = 8. The frequency of $[Ca^{2+}]_m$ oscillations in the antrum was not different from that observed in the corpus or in ICC cultured from the entire corpus and antrum ($P > 0.05$; Kruskal–Wallis 1-way ANOVA on ranks).

culture, and the corpus pacemakers entrain the antral pacemakers. Thus, this fundamental feature of gastric motility is reconstituted in cultured gastric ICC.

Gastric myoelectrical dysrhythmias occur in a wide variety of diseases and chronic conditions. Ectopic pacemakers with higher than normal frequencies in the antrums of these patients may delay gastric emptying[1] by reducing the strength of antral contractions (antral hypomotility)[10] and by impeding or totally blocking the normal orad to aborad spread of electrical slow waves.[5] In this study, we found that chronic defects in gastric ICC networks in W/W^V mice were associated with loss of the normal proximal-to-distal frequency gradient because of the emergence of higher frequency pacemaking in the antrum. This elevation in antral pacemaker frequency would tend to prevent corpus-to-antrum entrainment and reduce coupling between the corpus and the antrum, and this may contribute to the delayed gastric emptying observed in W/W^V mice.[27] Loss of the proximal-to-distal gastric frequency gradient also occurred in ICC from W/W^V stomachs. Thus, the change in intrinsic frequency in antral tissues appears to be due to a "reprogramming" of the pacemaker apparatus of antral ICC. Our data suggest that W/W^V mice and ICC derived from these animals may provide new models to study the effects of abnormal gastric pacemaking on gastric function and to investigate mechanisms responsible for alterations in gastric pacemaker frequency.

We recently studied ICC by light and electron microscopy in a murine model of human type 1 diabetes mellitus (nonobese diabetic mice).[26] There was a close correlation between disruptions in the ICC network and abnormalities in electrical slow wave activity in the antrums of these animals. Depletion of various classes of ICC and abnormalities in their ultrastructure have been described in several GI motility disorders that may, directly or indirectly, affect the gastric function (e.g., chronic and juvenile intestinal pseudo-obstruction, infantile hypertrophic pyloric stenosis, and diabetes).[23,32,38] However, it is difficult at the present time to correlate defects in ICC with gastric motility disorders because adequate histologic analyses have not been performed to evaluate gastric ICC (e.g., in pseudo-obstruction and diabetes). Our studies on mice have also shown that significant functional defects can arise in the stomach without total loss of ICC.[20,26] Therefore, significant defects in ICC networks might be missed in full-thickness biopsy specimens, in which one might find specimens with normal-appearing ICC and miss nonuniform changes in the ICC network that affect function. More thorough diagnostic techniques will be necessary to evaluate the density and distribution of ICC in functional gastric motility disorders.

W/W^V mice represent a virtually pure model of ICC depletion in the GI tract, because, aside from these cells, only mast cells appear to be affected.[24,25,39] There are 3 major classes of gastric ICC, and the present study demonstrates that, in addition to IC-IM[28] and IC-SM[29] cells, IC-MY networks are also significantly affected in W/W^V mice. Thus, involvement of all 3 classes of ICC may contribute to the electrical abnormalities observed in the present study. The most prominent change in stomachs of W/W^V mice is the virtually complete loss of IC-IM cells.[28] Despite the demonstrated dependence of all gastric ICC on Kit signaling,[20] gastric IC-MY cells remain in W/W^V mice.[28] This is probably because of differences in the sensitivity of the different classes of ICC classes to the reduced functionality of the tyrosine kinases encoded by the W and W^V alleles.[20] IC-IM are the primary targets of enteric motor innervation and mediate excitatory and inhibitory neurotransmission.[21,28] Therefore, it might be argued that loss of inhibitory innervation in the W/W^V antrum may cause an increase in intrinsic slow wave frequency. This is unlikely, however, because studies of isolated antral muscles have shown that neural blockade does not affect spontaneous pacemaker activity.[40] Second, the proximal-to-distal frequency gradient was maintained in cultured ICC in which ICC networks are not typically associated with neurons.

Recently, Dickens et al.[22] proposed that IC-IM may also be responsible for the secondary, regenerative component of the antral slow waves, at least in areas outside the greater curvature.[37] We also noticed that most slow waves in the W/W^V antrum lacked the fast ascending phase of depolarization, long plateaus, and spikes typical of electrical activity in this region (compare Figure 1*A* with Figure 7*A*). These changes rendered antral slow waves to be similar to the slow waves of the corpus. Thus, it is possible that the changes in waveform were due to the same effects that caused the increase in frequency. However, the notion that these changes must reflect the loss of IC-IM is based on the assumption that no other ICC classes are affected in the W/W^V stomach.[22,37] Data from the present study do not support this assumption. We found that both the density and the morphology of IC-MY networks are significantly altered in W/W^V stomachs, primarily in the corpus. Although our results do not eliminate the possibility that IC-IM loss contributes to the transformation of antral pacemakers to high-frequency oscillators, the findings of this study seriously question the utility of W/W^V mice as a "selective IC-IM knockout" as suggested by Dickens et al.[22]

Another ICC class that is affected by c-*kit* mutations is IC-SM. These ICC lie along the submucosal surface of the circular muscle layer.[29,36] Originally, these cells were only described in the pylorus,[29] but we consistently detected them throughout the antrums of Kit+/+ mice, except in the greater curvature. Horiguchi et al.[36] reported that cells near the submucosal surface, possibly IC-SM, have intrinsic pacemaker activity in the canine antrum. IC-SM may also function as pacemakers in the rodent stomach: Huang et al.[41] found that slow waves were preserved in guinea pig antral circular smooth muscle preparations that lacked IC-MY but contained part of the submucosa. However, it is difficult to envisage how loss of this morphologically quite sparse layer of ICC could result in an increase in the frequency of antral slow waves in W/W^V mice. The frequency of activity generated by pacemaker cells near the submucosa is either similar to[41] or much slower than the electrical rhythm produced by the dominant pacemaker IC-MY,[36] and faster oscillators entrain the activity of slower oscillators.[3,6,7]

The increase in slow wave frequency of the W/W^V antrum is likely to be due to a change in the intrinsic frequency of pacemaking by antral IC-MY. The mechanisms leading to this change are unclear, but it is remarkable that the frequency increase affects the region of the stomach in which IC-MY networks were the most preserved. "Corporalization" (i.e., an increase in intrinsic frequency) of antral pacemakers may represent an adaptive change in the pacemaker apparatus of IC-MY to the reduction in the pacemaking capability of the corpus.

To verify the hypothesis that the increased slow wave frequency in W/W^V antrums was due to altered activity of IC-MY, we assessed pacemaker activity of cultured ICC by monitoring $[Ca^{2+}]_m$ transients. As previously shown, oscillations in $[Ca^{2+}]_m$ are an index of pacemaker activity in ICC, and inhibitors of Ca^{2+} uptake block slow wave generation in gastric muscles.[33] Our results demonstrate that ICC cultured from the corpus and antrum of wild-type mice have distinct intrinsic frequencies. ICC cultured from Kit+/+ antrums displayed significantly slower intrinsic frequencies than corpus ICC, suggesting that pacemaker activity in the antrum is regulated in a different manner than in the corpus. Coculturing of corpus and antrum ICC typically resulted in entrainment of antral pacemakers to the higher frequency corpus rhythm. Thus, these experiments demonstrate that the frequency gradient fundamental to gastric peristalsis may be a basic feature of ICC, and coupling between regions of ICC may underlie the corpus-to- antrum entrainment typical of the intact stomach.[3,5–7] We have also verified these findings by directly monitoring slow wave depolarizations by imaging the fluorescence of the voltage-sensitive dye $DiBAC_4(3)$.[35] However, the corpus-to-antrum frequency gradient disappeared in IC-MY cultured from W/W^V antrums. The mechanisms of this change are not yet understood, but the loss of the frequency gradient was also manifest in intact gastric tissues (see above). In view of our finding that the frequency gradient is an intrinsic feature of ICC, it is likely that the changes in the W/W^V antrums are due to plasticity at the level of the IC-MY pacemaker apparatus.

The ectopic pacemaking in the W/W^V antrums was not associated with a significant shift in frequency toward tachy- or bradygastria. Rather, antral IC-MY converged on a rhythm that was close to the normal corpus frequency. This is consistent with our earlier finding that antrums of diabetic mice with depleted ICC networks had slow wave frequencies not significantly different than controls,[26] and similar frequency results were reported in rat models of type 1[42] and type 2 diabetes.[43] Raising antral frequency to levels close to the corpus frequency will tend to disrupt entrainment of antral pacemakers by the corpus (functional uncoupling). Loss of corpus-to-antrum entrainment because of breakdown of the gastric frequency gradient may be the dominant result of gastric dysrhythmias caused by disruption of ICC networks. This finding may have important diagnostic implications. Most clinical EGG laboratories rely primarily on frequency analysis and classification of recordings as brady-, normo-, or tachygastrias or arrhythmias (irregular dysrhythmias). Single-channel EGG measurements may miss the subtle, but physiologically relevant, changes in intrinsic antral frequency that may result in functional uncoupling of the corpus from the antrum. Multichannel EGG might be capable of detecting abnormal electrical activity if antral and corpus pacemakers run at different frequencies,[6] but, if functional uncoupling occurs without frequency dissociation, computer simulations have suggested that EGGs would contain unpredictable patterns at different electrode positions and a reduction in the dominant power in Fourier spectra.[44] This may make it difficult for the clinician using standard EGG analysis techniques to detect the kind of functional uncoupling predicted by equalization of antral and corpus pacemaker frequencies.[13,45]

In conclusion, we have previously established a link between disruptions in ICC networks and electrical dysrhythmias.[20] Our present findings strengthen this concept and provide further evidence that disruptions in ICC networks, which also occur in diabetes mellitus,[26,32] can result in the emergence of pacemakers that run at ele-

vated frequencies in the distal stomach. The enhancement in antral pacemaker frequency appears to be a fundamental reprogramming of the pacemaker mechanism in antral ICC, and it will be interesting to investigate the cause of this change. The rise in antral pacemaker frequency to the rate of corpus pacemaking results in a breakdown in the normal gastric frequency gradient. This will tend to disorganize gastric peristaltic contractions because the mechanical activity in the proximal and distal stomach is driven by competing pacemakers. Our data suggest that W/W^V mice are a potentially important new model for the study of new treatments of gastroparesis with underlying structural damage.

References

1. Camilleri M, Malagelada J-R, Brown ML, Becker G, Zinsmeister AR. Relation between antral motility and gastric emptying of solids and liquids in humans. Am J Physiol 1985;249:G580–G585.
2. Szurszewski JH. Electrical basis for gastrointestinal motility. In: Johnson LR, ed. Physiology of the gastrointestinal tract. 2nd ed. New York: Raven, 1987:383–422.
3. Kelly KA, Code CF. Canine gastric pacemaker. Am J Physiol 1971;220:112–118.
4. El-Sharkawy TY, Morgan KG, Szurszewski JH. Intracellular electrical activity of canine and human gastric smooth muscle. J Physiol (Lond) 1978;279:291–307.
5. Kim CH, Aziproz F, Malagelada J-R. Characteristics of spontaneous and drug-induced gastric dysrhythmias in a chronic canine model. Gastroenterology 1986;90:421–427.
6. Mintchev MP, Otto SJ, Bowes KL. Electrogastrography can recognize gastric electrical uncoupling in dogs. Gastroenterology 1997;112:2006–2011.
7. Chen, JDZ, Zou X, Lin X, Ouyang S, Liang J. Detection of gastric slow wave propagation from the cutaneous electrogastrogram. Am J Physiol 1999;277:G424–G430.
8. Chen JDZ, Pan J, McCallum RW. Clinical significance of gastric myoelectrical dysrhythmias. Dig Dis 1995;13:275–290.
9. Koch KL. Electrogastrography: physiological basis and clinical application in diabetic gastropathy. Diabetes Technol Ther 2001; 3:51–61.
10. You CH, Chey WY. Study of electromechanical activity of the stomach in humans and in dogs with particular attention to tachygastria. Gastroenterology 1984;86:1460–1468.
11. Dubois A. Gastric dysrhythmias: pathophysiologic and etiologic factors. Mayo Clin Proc 1989;64:246–250.
12. Sanders KM. Role of prostaglandins in regulating gastric motility. Am J Physiol 1984;247:G117–G126.
13. Jebbink RJA, Samsom M, Bruijs PPM, Bravenboer B, Akkermans LMA, VanBerge-Henegouwen GP, Smout AJPM. Hyperglycemia induces abnormalities of gastric myoelectrical activity in patients with type I diabetes mellitus. Gastroenterology 1994;107:1390–1397.
14. Walsh JW, Hasler WL, Nugent CE, Owyang C. Progesterone and estrogen are potential mediators of gastric slow wave dysrhythmias in nausea of pregnancy. Am J Physiol 1996;270:G506–G514.
15. Kim MS, Chey WD, Owyang C, Hasler WL. Role of plasma vasopressin as a mediator of nausea and gastric slow wave dysrhythmias in motion sickness. Am J Physiol 1997;272:G853–G862.
16. Debinski HS, Ahmed S, Milla PJ, Kamm MA. Electrogastrography in chronic intestinal pseudoobstruction. Dig Dis Sci 1996;41: 1292–1297.
17. Thor PJ, Kolasinska-Kloch W, Pitala A, Janik A, Kopp B, Sibiga W. The influence of aging on autonomic nervous system activity and gastric myoelectric activity in humans. Folia Med Cracov 1999; 40:53–62.
18. Koch KL. Diabetic gastropathy. Gastric neuromuscular dysfunction in diabetes mellitus. A review of symptoms, pathophysiology, and treatment. Dig Dis Sci 1999;44:1061–1075.
19. Dickens EJ, Hirst GDS, Tomita T. Identification of rhythmically active cells in guinea-pig stomach. J Physiol (Lond) 1999;514: 515–531.
20. Ördög T, Ward SM, Sanders KM. Interstitial cells of Cajal generate electrical slow waves in the murine stomach. J Physiol (Lond) 1999;518:257–269.
21. Ward SM, Sanders KM. Interstitial cells of Cajal: primary targets of enteric motor innervation. Anat Rec 2001;262:125–135.
22. Dickens EJ, Edwards FR, Hirst GDS. Selective knockout of intramuscular interstitial cells reveals their role in the generation of slow waves in mouse stomach. J Physiol (Lond) 2001;531:827–833.
23. Sanders KM, Ördög T, Koh SD, Torihashi S, Ward SM. Development and plasticity of interstitial cells of Cajal. Neurogastroenterol Motil 1999;11:311–338.
24. Ward SM, Sanders KM. Physiology and pathophysiology of the interstitial cell of Cajal: from bench to bedside I. Functional development and plasticity of interstitial cells of Cajal networks. Am J Physiol 2001;281:G602–G611.
25. Huizinga JD. Physiology and pathophysiology of the interstitial cell of Cajal: from bench to bedside II. Gastric motility: lessons from mutant mice on slow waves and innervation. Am J Physiol 2001;281:G1129–G1134.
26. Ördög T, Takayama I, Cheung WKT, Ward SM, Sanders KM. Remodeling of networks of interstitial cells of Cajal in a murine model of diabetic gastroparesis. Diabetes 2000;49:1731–1739.
27. Der-Silaphet T, Malysz J, Hagel S, Arsenault AL, Huizinga JD. Interstitial cells of Cajal direct normal propulsive contractile activity in the mouse small intestine. Gastroenterology 1998;114: 724–736.
28. Burns AJ, Lomax AEJ, Torihashi S, Sanders KM, Ward SM. Interstitial cells of Cajal mediate inhibitory neurotransmission in the stomach. Proc Natl Acad Sci U S A 1996;93:12008–12013.
29. Ward SM, Morris G, Reese L, Wang X-Y, Sanders KM. Interstitial cells of Cajal mediate enteric inhibitory neurotransmission in the lower esophageal and pyloric sphincters. Gastroenterology 1998;115:314–329.
30. Kim TW, Beckett EAH, Hanna R, Koh SD, Ördög T, Ward SM, Sanders KM. Regulation of pacemaker frequency in the murine gastric antrum. J Physiol (Lond) 2002;538:145–157.
31. Nocka K, Tan JC, Chiu E, Chu TY, Ray P, Traktman P, Besmer P. Molecular bases of dominant negative and loss of function mutations at the murine c-kit/white spotting locus: W^{37}, W^{v}, W^{41}, and W. EMBO J 1990;9:1805–1813.
32. He C-L, Soffer EE, Ferris CD, Walsh RM, Szurszewski JH, Farrugia G. Loss of interstitial cells of Cajal and inhibitory innervation in insulin-dependent diabetes. Gastroenterology 2001;121:427–434.
33. Ward SM, Ördög T, Koh SD, Abu Baker S, Jun JY, Amberg G, Monaghan K, Sanders KM. Pacemaking in interstitial cells of Cajal depends upon calcium handling by endoplasmic reticulum and mitochondria. J Physiol (Lond) 2000;525:355–361.
34. Trollinger DR, Cascio WE, Lemasters JJ. Mitochondrial calcium transients in adult rabbit cardiac myocytes: inhibition by ruthenium red and artifacts caused by lysosomal loading of Ca^{2+}-indicating fluorophores. Biophys J 2000;79:39–50.
35. Stevens T, Cornfield DN, McMurtry IF, Rodman DM. Acute reductions in PO_2 depolarize pulmonary artery endothelial cells and decrease $[Ca^{2+}]_i$. Am J Physiol 1994;266:H1416–H1421.

36. Horiguchi K, Semple GSA, Sanders KM, Ward SM. Distribution of pacemaker function through the tunica muscularis of the canine gastric antrum. J Physiol (Lond) 2001;537:237–250.
37. Hirst GDS, Beckett EAH, Sanders KM, Ward SM. Regional variation in contribution of myenteric and intramuscular interstitial cells of Cajal to generation of slow waves in mouse gastric antrum. J Physiol (Lond) 2002;540:1003–1012.
38. Vanderwinden J-M, Rumessen JJ. Interstitial cells of Cajal in human gut and gastrointestinal disease. Microsc Res Tech 1999;47:344–360.
39. Ward SM, Burns AJ, Torihashi S, Sanders KM. Mutation of the proto-oncogene c-kit blocks development of interstitial cells and electrical rhythmicity in murine intestine. J Physiol (Lond) 1994; 480:91–97.
40. El-Sharkawy TY, Szurszewski JH. Modulation of canine antral circular smooth muscle by acetylcholine, noradrenaline and pentagastrin. J Physiol (Lond) 1978;279:309–320.
41. Huang S-M, Nakayama S, Iino S, Tomita T. Voltage sensitivity of slow wave frequency in isolated circular muscle strips from guinea pig gastric antrum. Am J Physiol 1999;276:G518–G528.
42. Xue L, Suzuki H. Electrical responses of gastric smooth muscles in streptozotocin-induced diabetic rats. Am J Physiol 1997;272: G77–G83.
43. Takano H, Imaeda K, Koshita M, Xue L, Nakamura H, Kawase Y, Hori S, Ishigami T, Kurono Y, Suzuki H. Alteration of the properties of gastric smooth muscle in the genetically hyperglycemic OLETF rat. J Auton Nerv Syst 1998;70:180–188.
44. Liang J, Chen JDZ. What can be measured from surface electrogastrography. Dig Dis Sci 1997;42:1331–1343.
45. Jebbink HJA, Bruijs PPM, Bravenboer B, Akkermans LMA, van-Berge-henegouwen GP, Smout AJPM. Gastric myoelectrical activity in patients with type I diabetes mellitus and autonomic neuropathy. Dig Dis Sci 1994;39:2376–2383.

Received March 13, 2002. Accepted August 29, 2002.

Address requests for reprints to: Kenton M. Sanders, Ph.D., Department of Physiology and Cell Biology, University of Nevada, Reno School of Medicine, Anderson Bldg./352, Reno, Nevada 89557; e-mail: kent@physiology.unr.edu; fax: 775-784-6903.

Supported in part by National Institutes of Health grant DK40569 (to K.M.S.) and a Research Grant Award from the American Motility Society and Janssen Pharmaceutica and Research Foundation (to T.Ö.). A core laboratory supported by DK41315 provided support for the morphologic studies.

T. Ördög and M. Baldo share first authorship on this paper.

The authors thank Nancy N. Horowitz for expert technical assistance and Chris Steadham, Digital Imaging Consultant, JH Technologies, San Jose, California, for the image shown in Figure 3.